Pharmaceutical Research (2022) 39:2699–2707
https://doi.org/10.1007/s11095-022-03398-5

ORIGINAL RESEARCH ARTICLE

Formulation of Lipid-Free Polymeric Mesoscale Nanoparticles Encapsulating mRNA

Rachel Skelton[1] · Arantxa Roach[1] · Lauren E. Prudhomme[1] · Jing Yu Carolina Cen Feng[1] · Pooja Gaikwad[1,2] · Ryan M. Williams[1,2]

Received: 15 May 2022 / Accepted: 14 September 2022 / Published online: 26 September 2022
© The Author(s), under exclusive licence to Springer Science+Business Media, LLC, part of Springer Nature 2022

Abstract

Introduction Nanoparticle-mediated gene therapy has found substantial clinical impact, primarily focused on lipid-based nanoparticles. In comparison with lipid nanoparticles, polymeric particles may have certain advantages such as increased biocompatibility and controlled release. Our prior studies have found that polymeric mesoscale nanoparticles exhibited specific targeting to the renal proximal tubules. Thus, in this study, we sought to identify formulation parameters that allow for development of polymeric mesoscale nanoparticles encapsulating functional mRNA for delivery into tubular epithelial cells.
Methods We evaluated particle uptake *in vitro* prior to exploring formulation parameters related to introduction of a primary mixture of polymer in acetonitrile and hydrophilic mRNA in water. Finally, we evaluated their functionality in a renal tubular epithelial cell line.
Results We found that MNPs are endocytosed within 15 min and that the mesoscale nanoparticle formulation procedure was generally robust to introduction of a primary mixture and encapsulation of mRNA. These particles exhibited substantial uptake in renal cells *in vitro* and rapid (< 1 h) expression of a model mCherry fluorescent protein.
Conclusion We anticipate these findings having potential in the delivery of specific gene therapies for renal disorders and cancer.

Keywords gene delivery · kidney disease · mRNA · polymeric nanoparticles · translation

Introduction

Nanomedicine-based formulations of gene therapies have found increased clinical utility within the past decade [1–3]. Clinically-approved nanomedicines include siRNA lipid nanoparticle formulations developed by Alnylam Pharmaceuticals [2, 4], with Patisiran initially approved by the US FDA in 2018 [4, 5]. The most well-known examples are mRNA lipid nanoparticle formulations as vaccines against SARS-Cov-2, gaining FDA emergency use authorization in 2020 [6–9]. Beyond these, mRNA therapeutics have increasingly shown potential in the lab and clinic [10, 11].

These successes have spurred significant advances in research related to systems for delivery of mRNA, siRNA, DNA plasmids, CRISPR components, and others [1, 9, 12–14]. The most advanced and widely-used formulations are lipid-based [2, 3, 15, 16]. There has additionally been substantial work in developing polymeric gene delivery nanoformulations [17, 18]. The majority of these integrate ionizable lipids or cationic polymers to increase loading of the active pharmaceutical ingredient [16, 19]. Lipid nanoparticle gene delivery systems may have drawbacks related to their controlled release, while cationic polymer systems may exhibit some toxicity related to their interactions with negatively-charged cell plasma membranes [14, 17, 20]. Substantial work has investigated the formulation of small molecules within polymeric nanoparticles, however few recent studies have investigated gene delivery with polymer delivery systems [20–22].

In prior studies, we formulated mesoscale nanoparticles (MNPs) made from diblock co-polymers poly(lactic-*co*-glycolic) acid conjugated to polyethylene glycol (PLGA-PEG) [23]. Such MNPs demonstrated substantial kidney

Rachel Skelton and Arantxa Roach contributed equally.

✉ Ryan M. Williams
rwilliams4@ccny.cuny.edu

[1] Department of Biomedical Engineering, The City College of New York, New York, NY 10031, USA

[2] PhD Program in Chemistry, Graduate Center, City University of New York, New York, NY 10016, USA

targeting, up to 26-fold more than other organs, with preferential localization into renal proximal tubular epithelial cells *via* transcytosis across the peritubular endothelium [24]. In prior studies we have formulated such MNPs to encapsulate small molecule dyes [24] and reactive oxygen species scavengers [25] using nanoprecipitation while evaluating their therapeutic or imaging efficacy *in vivo*. We have also formulated short oligonucleotides [26], such as siRNA [27, 28], as well as peptides [29, 30], using a primary mixture-nanoprecipitation method. We found that MNPs with these various cargoes retain renal targeting and exhibit therapeutic efficacy against both acute and chronic kidney disease. In this work, we sought to adapt this method and optimize it to evaluate the encapsulation and functionality of mRNA within polymeric MNPs, with no lipid or polycationic components. We used an mCherry mRNA as a model fluorescent protein-encoding transcript, as well as traditional fluorophore formulations to evaluate intracellular uptake and localization of these particles.

Methods

Formulation of Dye-Loaded Mesoscale Nanoparticles (MNPs)

Mesoscale nanoparticles loaded with the fluorescent dye 3,3'-diethylthiadicarbocyanine iodide (DEDC) were formulated as previously described [23, 24]. Briefly, a di-block copolymer consisting of 38–54 kDa poly(lactic-*co*-glycolic acid) (PLGA) (Sigma; St. Louis, MO) conjugated to 5 kDa acid-terminated polyethylene glycol (PEG) (Nanocs; New York, NY) was prepared *via* carbodiimide chemistry, precipitated, and dried under vacuum. This served as the basis for MNP formulation, wherein 100 mg diblock copolymer was dissolved in 2 mL acetonitrile (Sigma). For dye-loaded MNPs, DEDC (Fisher Scientific; Hampton, NH), 10 mg dye was co-dissolved in the acetonitrile solution, which was added dropwise *via* syringe pump at a rate of 0.1 mL/minute to a solution of 4 mL purified water and 100 µL Pluronic F-68 (Fisher Scientific) under moderate stirring in a round-bottom flask. After addition, the solution was stirred for 100 additional minutes for MNP solidification. This suspension was then centrifuged at 7,400 X g for 15 min, washed with 10 mL deionized water and re-pelleted. The particles were resuspended in 10 mL 2% sucrose, flash-frozen, and lyophilized until a light powder was formed (48–72 h) and stored at -20°C until use. Separately, an empty MNP control was made with an identical formulation, omitting the DEDC addition(Table I). This empty MNP control served as a baseline comparison to the original formulation without interference of overlapping dye fluorescence.

Table I Physicochemical Characteristics of Dye or Empty MNPs

Particle	Hydrodynamic Diameter (nm)	PDI	ζ-potential (mV)	Loading (µg/mg particle)
Nanoprecipitation DEDC MNPs	407.9 ± 5.7	0.27	-30.0 ± 0.7	1.1
Two-step Nanoprecipitation DEDC MNPs	415.7 ± 8.2	0.17	-21.0 ± 1.4	0.34
Empty MNPs	333.3 ± 6.5	0.33	-26.0 ± 0.2	–

In Vitro Uptake of Dye-Loaded MNPs

In order to determine the uptake kinetics and subcellular localization of MNPs in general, we used a dye-loaded MNP [23, 24]. Uptake was evaluated in the 786-O renal tubular epithelial cell adenocarcinoma line (American Type Culture Collection; Manassas, VA). Cells were cultured with complete growth medium, including RPMI-1640 (Fisher) + 10% fetal bovine serum (Fisher) + Primocin antibiotic/antimycotic additive (Invivogen; San Diego, CA) under 5% carbon dioxide with humidity at 37°C. Cells were cultured in T75 culture flasks with approximately weekly subculturing and bi-weekly media changes, and subcultured into 24-well culture dishes prior to microscopy experiments. Microscopy was performed on an EVOS M5000 (Fisher) inverted digital microscope with filter sets: DAPI (Ex/Em: 357/447 nm); GFP (470/510 nm); RFP (531/593 nm); Cy5 (628/692 nm). Images were captured and analyzed on ImageJ software using mean intensity per cell area [31].

For time-course studies, cells were incubated with 1 mg/mL DEDC-MNPs in culture for up to one hour, with different wells imaged at 15, 30, 45, and 60 min. Separately, wells were incubated with an equal amount of DEDC dye alone as compared to that within MNPs (1 µg/mL) to determine differential uptake related to the MNPs, as well as a PBS-only control. At each timepoint, media/particle suspension was removed, washed, and PBS was added to the well for imaging. Analyses were performed on 6 images per condition over multiple wells using ImageJ for mean fluorescence per area, with mean ± standard deviation determined for each condition and timepoint. For subcellular localization studies, cells were incubated with Hoechst 33342 to stain nuclear DNA (DAPI channel) (Fisher) and MemBrite to stain the cell membrane (GFP channel) (Biotium; Fremont, CA) according to manufacturer's instructions, and with 10 µg/mL DEDC-MNPs for one hour. A lower concentration was used to be able to

visualize other dyes clearly. Following incubation, media was removed, cells were washed, and PBS was added to the well for imaging. Simultaneously, cells were incubated with DEDC-MNPs for one hour.

Formulation of mRNA-Loaded MNPs

Formulation of MNPs proceeded similarly to as above with several variations. We first modulated the parameters of a primary homogenous mixture system prior to nanopreciptation in order to investigate their effects on the ability to formulate mesoscale nanoparticles between 300–425 nm, taking advantage of the miscibility of acetonitrile in water [23, 24]. Briefly, 100 mg PLGA-PEG was dissolved in 2 mL acetonitrile. To modulate the primary mixture, we added either 5 or 10 µg of EZCap mCherry mRNA (ApexBio; Houston, TX) in 10, 20, 100, or 500 µL of RNAse-free water (Fisher) (Table II). The homogenous mixture was formed by mRNA addition dropwise under agitation on a vortex at 25% power. This mixture was drawn into a 10 mL glass syringe and added dropwise (0.1 mL / minute) *via* syringe pump to a solution of 4 mL RNAse-free purified water and 100 µL Pluronic F-68. This nanoprecipitation step was conducted in a round-bottom flask on a stir plate under moderate stirring, which continued for 100 min following addition of the mRNA mixture. The particle suspension was centrifuged as above and washed once with 10 mL RNAse-free water prior to resuspension in an RNAse-free 2% sucrose solution and flash-frozen. The resuspended particles were lyophilized as above for 48 h until a light powder was formed. This lyophilized particle formulation was sealed to prevent moisture aggregation and stored at -20°C until use.

We also sought to compare this two-step MNP formulation process used for mRNA with the above DEDC single-step formulation process (Table I). To do so, 10 mg DEDC dye as above was dissolved in 2 mL acetonitrile and a primary homogenous mixture was formed with 10 µL water as in the optimized mRNA formulation. All other formulation parameters were similar between the two processes.

MNP Encapsulation and Physicochemical Characterization

The physicochemical characteristics of all MNPs were evaluated *via* a NanoZS90 (Malvern Panalytical; Malvern, UK). Mesoscale nanoparticle hydrodynamic diameter and polydispersity index were evaluated *via* dynamic light scattering, and ζ-potential was evaluated *via* electrophoretic light scattering. To determine loading of the small molecule fluorescent dye DEDC, a 1 mg/mL suspension of dye-loaded MNPs in 1×PBS was loaded in a UV–Vis spectrophotometer (Jasco; Easton, MD) and absorbance was measured at 650 nm. To determine loading of the mRNA, MNPs containing mCherry mRNA were first dissolved in acetonitrile and Tris–EDTA buffer, then centrifuged to pellet the polymer at 31,300 X g for 30 min. The supernatant which contained freed mRNA was subjected to QuantIT RiboGreen RNA quantification kit per manufacturer's instructions (Fisher). Release of the mRNA was performed in triplicate by incubating mRNA-MNPs in 10% fetal bovine serum (FBS) either at room temperature or 37°C. At timepoints of 2, 4, 6, 24, 48, and 72 h, the particles were centrifuged at 7,400×g, and the supernatant was subjected to the QuantIT assay as above. Remaining mRNA to total 100% was recovered from particles leftover after centrifugation at 72 h as above. Atomic force microscopy was performed *via* a Bruker Multimode 8 AFM in tapping mode in air.

Evaluation of mRNA Expression *In Vitro via* Fluorescence Microscopy

To evaluate the functionality of mCherry mRNA MNPs, the optimal formulation (#1 from Table II) was introduced to cells in culture. Briefly, in triplicate, 1 or 10 mg/mL MNPs suspended in complete cell culture media was added to 786-O cells in a 24-well plate at near-confluence. MNPs were allowed to incubate under normal cell growth conditions for 1 h, 4 h, or 24 h after addition. Cells were imaged using the EVOS fluorescence microscope under the RFP filter and transmitted light at each timepoint in several locations. Control experiments included: 786-O cells incubated with no MNPs at the same growth phase as above; 786-O cells incubated with empty MNPs for 24 h; and mCherry mRNA MNPs incubated in complete cell growth media with no 786-O cells.

Table II Primary Mixture Parameters and mRNA-MNP Characteristics

Batch	mRNA Mass (µg)	Volume of mRNA solution (µL)	Hydrodynamic Diameter (nm)	PDI	ζ-potential (mV)
1	10	10	392.7 ± 25	0.37	-22.9 ± 0.5
2	10	20	330.1 ± 5.8	0.31	-31.4 ± 1.5
3	10	100	311.7 ± 4.8	0.17	-29.8 ± 0.5
4	10	500	254.7 ± 3.6	0.13	-30.5 ± 0.1
5	5	10	342.4 ± 5.2	0.21	-21.9 ± 0.7

All imaging conditions controlled for light exposure and gain across wells and images. Images were processed using ImageJ—all RFP filter images were set to the same max/min brightness settings for visualization. For quantification, regions of interest (ROIs) were manually drawn around 20 cells per condition using the transmitted light image, transferred to the RFP image, and measured as mean signal. Mean/standard deviation of cell measurements were obtained and compared to the no-MNP control. The mean fluorescence signal from control cells was subtracted from each cell to correct for background signal. Mean and standard deviations of the normalized signal from each condition were obtained, and the proportion of positive cells was defined as those with signal above background. Normalized fluorescence signal per cell was analyzed *via* two-way analysis of variance (ANOVA) using Origin Pro 2020 (Origin Lab Corp, Northampton, MA) with factors of incubation time and MNP concentration, followed by a Tukey multiple comparison's test.

Evaluation of mRNA Expression *In Vitro via* Automated Image-Based Cytometry

We additionally performed mCherry expression assays using automated image-based cytometry. Duplicate wells of 786-O cells under each condition were plated in 6-well plates. One set of experiments evaluated cells after incubation with 1 mg/mL mCherry mRNA MNPs, 1 mg/mL empty MNPs, and an equal volume of PBS. Another set of experiments evaluated cells after incubation with 10 mg/mL mCherry mRNA MNPs, 10 mg/mL MNPs, and an equal volume of PBS. Cells were incubated with the above for 15 min, 30 min, 1 h, 2 h, or 24 h. Following incubation, cells were washed once with PBS and fixed with 10% neutral buffered formalin (Fisher) for 30 min and washed again. Cells were scraped and subjected to automated image-based cytometry using a Countess II (Fisher) outfitted with a RFP filter cube. A size threshold of 10—50 µm was imposed for automated cell identification via brightfield images. RFP channel brightness was obtained as average RFU for 4–6 images obtained per treatment condition. Cell concentrations were determined to be a minimum of 10^5/mL, with approximately 100 cells analyzed per imaging field. An average of autofluorescence per condition was obtained (PBS-treated cells) and subtracted from each image average RFU, which were then plotted as mean ± deviation for each timepoint/condition.

Results

Uptake of MNPs in 786-O Cells

To evaluate the differential uptake of DEDC into 786-O cells renal epithelial carcinoma cells, whether as a free dye or encapsulated inside MNPs, we formulated an MNP loaded with a Cy5 fluorescent dye (DEDC) and evaluated intracellular fluorescence up to 60 min.. DEDC-MNPs exhibited a hydrodynamic diameter of 407.9 ± 5.7 nm, a PDI of 0.27, and zeta potential of -30.0 ± 0.7 mV (Table I). They were loaded with 1.1 µg DEDC/mg MNP. We first evaluated uptake over time and found that within 15 min, MNPs were internalized into the cells compared to PBS controls (Fig. 1a-c), which did not significantly increase up to one hour (Fig. 1d). We found that little, if any, fluorescence above background was observed in cells incubated with DEDC dye alone (Fig. 1b, d). At one hour, each cell appears to have MNP uptake with punctate spots and some diffuse localization (Fig. 1c, d). Upon co-staining cells with a cell membrane dye and nuclear dye, we found that the particles were internalized into the cell membrane and located to the perinuclear region within one hour as evaluated by colocalization of fluorescence from the dye and comparison to a nuclear and cell membrane dyes. (Fig. 2).

mCherry mRNA MNP Formulation

Five separate formulations of mesoscale nanoparticles encapsulating mCherry mRNA were prepared. To ensure that the formulation matched parameters of mesoscale nanoparticles (300–425 nm in diameter) and maintained renal localization *in vivo* [23, 24], we investigated parameters of a homogenous primary mixture of mRNA in acetonitrile prior to nanoprecipitation. Of the five formulations, four exhibited appropriate sizes within this range, and just one—the extreme high value of mRNA dilution—exhibited an out-of-range size of 254.7 nm (Table II). The formulation which most closely matched the DEDC-MNP formulation above, and that which was also the most straightforward was formulation 1, which involved use of the 1 mg/mL mCherry mRNA stock solution without dilution. Formulations 2–5 involved dilution of the stock 2X, 10X, and 50X, and interestingly, all sizes below 350 nm. Each also exhibited a lower PDI than formulation 1, likely related to the size reduction. Prior studies demonstrated that in addition to the size parameters above, a PDI of < 0.4 is acceptable for MNP-based renal targeting efficiency [23, 24]. Finally, all formulations exhibited a ζ-potential between -22 and -31 mv, within mesoscale formulation parameters [23, 24].

As all five particle formulations exhibited appropriate PDI and charge parameters, and four of five exhibited appropriate sizing, that with the closest to the DEDC-MNP size and the simplest formulation was chosen for further study (formulation 1 due to no dilution step) to facilitate future scale-up. This formulation exhibited a hydrodynamic diameter of 392.7 ± 25 nm with a

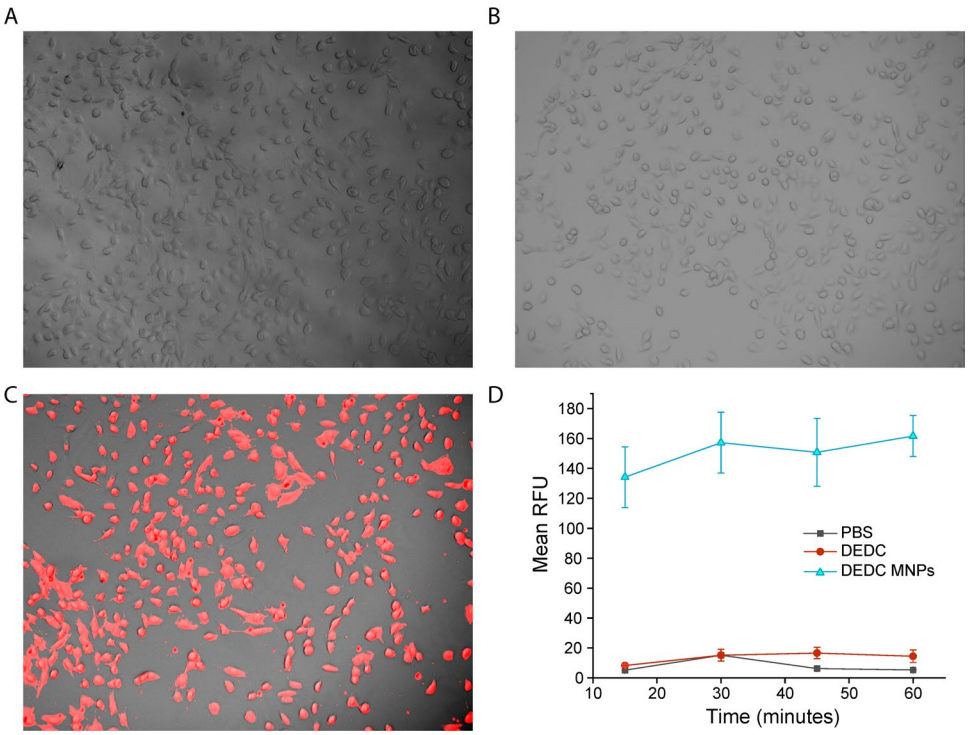

Fig. 1 Uptake of fluorescent dye-loaded MNPs in 786-O cells. (**A**) Transmitted light and Cy5 fluorescence of 786-O cells incubated with PBS for 15 min imaged at 100X. (**B**) Transmitted light and Cy5 fluorescence of 786-O cells incubated with 1 µg/mL DEDC dye alone for 15 min imaged at 100X. (**C**) Transmitted light and Cy5 fluorescence of 786-O cells incubated with 1 mg/mL DEDC MNPs for 15 min imaged at 100X. (**D**) Normalized Cy5 signal from 786-O cells after incubation for up to one hour in 15-min increments. Each point represents mean ± standard deviation of six images.

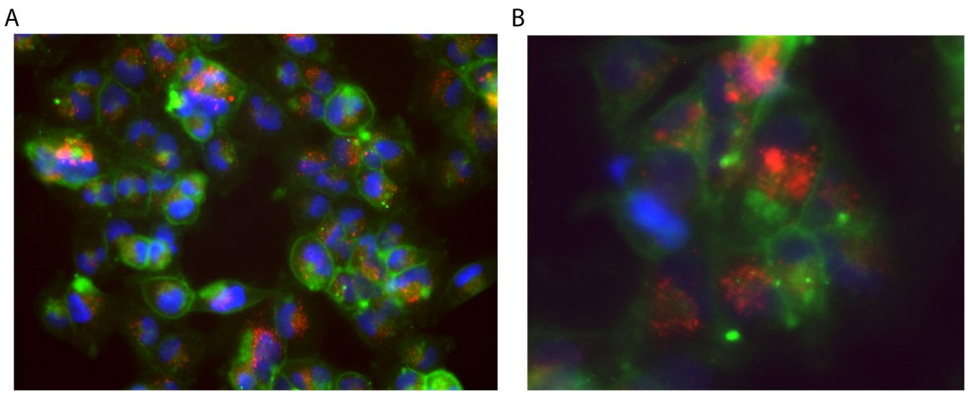

Fig. 2 Subcellular localization of fluorescent dye-loaded MNPs in 786-O cells. (**A**) Subcellular localization of DEDC-MNPs in 786-O cells at 200X and (**B**) 400X. Green: MemBrite cell membrane dye; Blue: Hoechst nuclear dye; Red: Cy5 encapsulated within MNPs.

polydispersity index of 0.37. The formulation encapsulated 18.1 ng mRNA per 1 mg MNP. This represents an encapsulation efficiency of approximately 45%. Additionally, *via* atomic force microscopy (AFM) we found a generally spherical morphology with some dispersity as expected from the PDI above, while the particles were generally within the size range expected (with some slight shrinkage accounted for as particles were analyzed *via* dry AFM) (Fig. 3a). Further, we evaluated the release of mRNA from the MNPs in 10% FBS at room temperature and at 37°C, finding that about 15% of the mRNA is released within 2 h, about 50% within 6 h, and up to approximately 90% is released more slowly up to 72 h (Fig. 3b).

Uptake and Expression of mCherry mRNA in 786-O Cells

In order to evaluate the functional expression of mCherry mRNA in 786-O renal cell carcinoma epithelial cells, we incubated mRNA-encapsulating MNPs *in vitro* for varying time periods. First, a 1 mg/mL suspension in complete cell media was used to evaluate uptake and expression at low levels of MNP (Fig. 4). Within just one hour of incubation, the cell culture exhibited low levels of mRNA expression (Fig. 4a). At 4 h, the expression of mCherry protein appeared to increase slightly, however images at 24 h appeared similar to those at one hour. We quantified expression of mCherry per cell and found that there were no significant differences

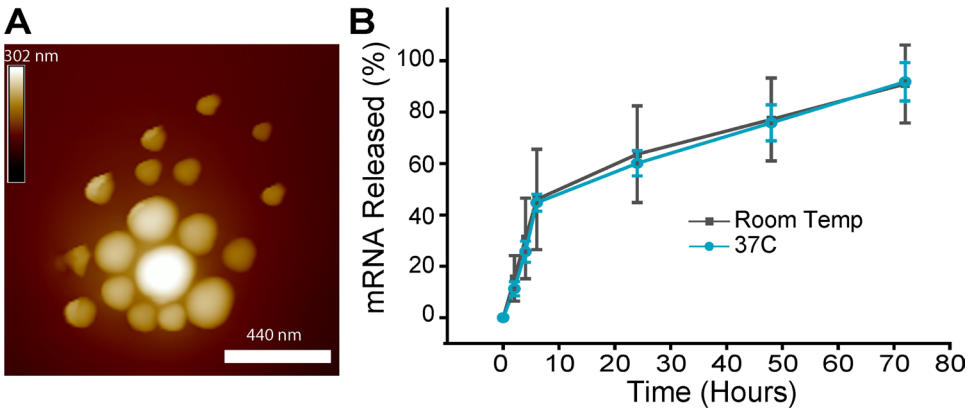

Fig. 3 Characterization of mCherry mRNA-MNPs. (**A**) Atomic force microscopy of a region of mRNA-MNPs. (**B**) Release of mRNA from MNPs up to 72 h in 10% FBS either at room temperature or at 37°C. Data points represent mean ± standard deviation of 3 replicates.

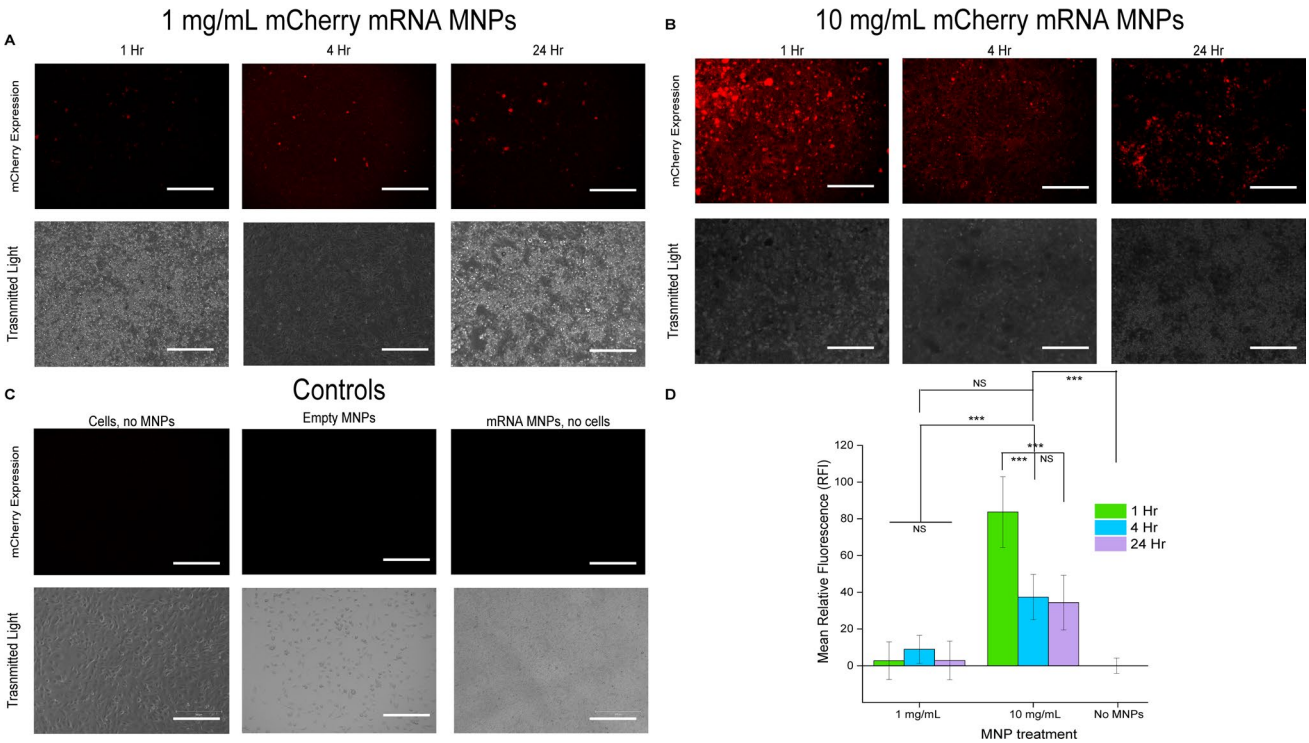

Fig. 4 Expression of mCherry mRNA after intracellular delivery by MNPs. (**A**) 1 mg/mL of mCherry mRNA-MNPs was incubated with 786-O renal tubular epithelial cells for 1, 4, and 24 h. Top row: RFP filter; Bottom row: transmitted light. (**B**) 10 mg/mL of mCherry mRNA-MNPs were incubated the same as in Panel A. (**C**) Control experiments of 786-O cells treated with no MNPs or empty MNPs (left, center respectively) for 24 h or imaging of mCherry mRNA MNPs with no cells present (right). Scale bar = 300 µm. (**D**) Mean relative fluorescence was obtained from each timepoint and concentration treatment of mCherry mRNA MNPs with 786-O cells and compared for 20 ROIs per image. NS = not significant; *** = $p < 0.05$.

among any of the timepoints (Fig. 4d). It should also be noted that fluorescence expression was not significantly different on a per-cell basis compared to the control cells with no MNPs. However, this is likely because only a proportion of cells appeared to have uptake. At one hour, just 60% of cells exhibited mCherry fluorescence, whereas at 4 h it was 90%, though expression was returned to just 55% of cells at 24 h. Interestingly, transmitted light images of near-confluent wells appeared to show some darkening or haziness due to the large size of MNPs.

We next evaluated 786-O cell expression of mCherry mRNA at an MNP concentration of 10 mg/mL suspended in complete cell media. Within just one hour of incubation, we observed substantial expression of mCherry, approximately 40-fold higher than the same timepoint with a 1 mg/mL MNP concentration (Fig. 4b). Though expression was maintained at 4 and 24 h, it did appear somewhat diminished at approximately half the total mean fluorescence as the one hour timepoint, a difference which was statistically significant (Fig. 4d). All cells that were analyzed exhibited some

level of mCherry expression. We found this expression was significantly higher compared to the 1 mg/mL incubation and compared to the control cells incubated with no MNPs (Fig. 4d).

To ensure visualized fluorescence was indeed emanating from expressed mCherry protein, we performed several controls (Fig. 4c). First, we imaged cells in the same growth phase with no MNPs and visualized no background fluorescence (Fig. 3). We next performed imaging on 786-O cells incubated with empty MNPs (333.3 ± 6.5 nm; PDI 0.33; -26.0 ± 0.2 mV) to serve as a no-fluorescence control and comparison to the original MNP formulation. Again, we found no fluorescence in the mCherry channel. Finally, we performed imaging with mCherry mRNA-MNPs in the absence of 786-O cells. Here, interestingly again, we were able to visualize the MNPs *via* transmitted light microscopy, though no mCherry fluorescence was observed.

To further quantify and confirm the expression of mCherry from cells treated with mCherry mRNA MNPs, we performed automated image-based fluorescence cytometry. 786-O cells treated with either 1 mg/mL or 10 mg/mL mCherry mRNA MNPs were compared to cells treated with an equal amount of empty MNPs or an equal volume of PBS. As found with fluorescence microscopy, these studies demonstrated that the 1 mg/mL concentration exhibited some increase above background, though it was within variation, within 1 h, which increased at 2 h and decreased at 24 h (Fig. 5a). With incubation of 10 mg/mL MNPs, we again found an increase in fluorescence intensity at 1 h, which plateaued at 2 h and decreased at 24 h (Fig. 5b). In neither set of experiments did we see substantial expression of mCherry above background at either 15 or 30 min of incubation. It should be noted that we did not see several-fold enhancement with the 10 mg/mL in these studies as we did in fluorescence microscopy experiments, potentially stemming from fixation or from limitations in dynamic range of the detector compared to microscopy. However, these studies do further support that expression of mCherry mRNA delivered by MNPs into renal proximal tubule cells is achievable within 1 h and sustainable up to 24 h.

Discussion

In this study, we sought to evaluate the formulation parameters of a polymeric nanoparticle encapsulating mRNA for targeted gene delivery. The goal was to maintain mesoscale nanoparticle size in the 300–425 nm hydrodynamic diameter range while modifying the formulation system to incorporate an acetonitrile:water mixture step for large nucleic acid cargoes [23, 24]. We found that overall, the physicochemical characteristics of resultant particles were robust to incorporation of the mRNA mixture step, and that the mesoscale nanoparticles were able to deliver functional mCherry mRNA into a renal tubular epithelial cell line.

We first evaluated the uptake kinetics of these particles within this cell line and their subcellular localization to determine the timing of imaging studies with mCherry mRNA. We found that indeed these particles were endocytosed into the renal tubular epithelial cells in just 15 min and localized to the perinuclear region of the cells [32], consistent with endolysosomal trafficking and escape as previously found for PLGA nanoparticles, portending possible gene delivery [33]. This evidence that MNPs are rapidly endocytosed into the 786-O renal tubular epithelial adenocarcinoma cell line suggests they may be amenable to gene delivery.

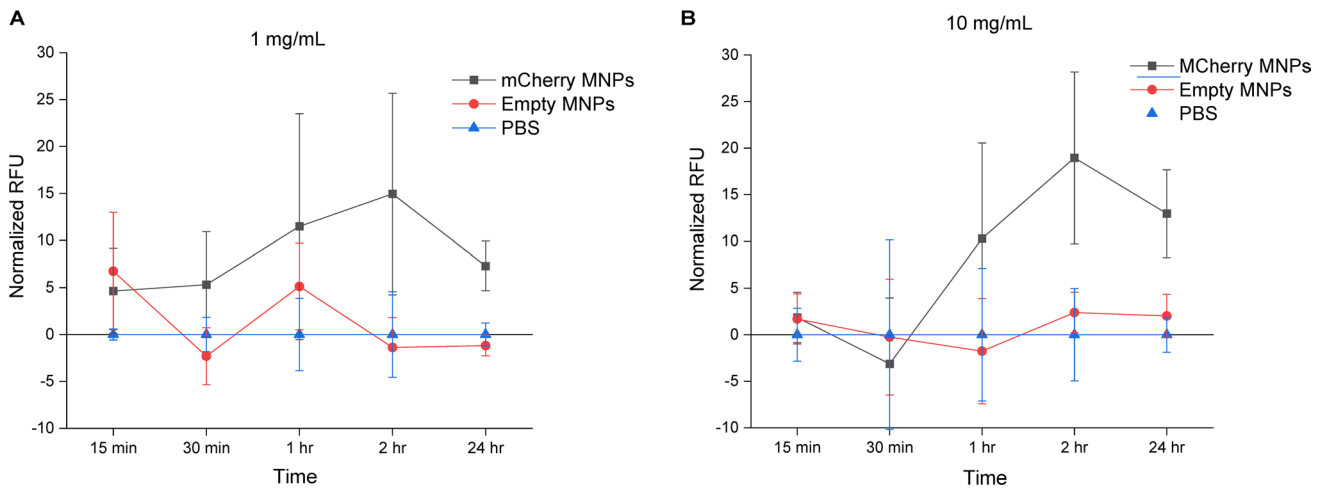

Fig. 5 Quantification of mCherry expression in 786-O cells via automated image-based cytometry. (**A**) Normalized relative fluorescence units (RFU) obtained from 4–6 automated images in cells treated with 1 mg/mL mCherry MNPs or Empty MNPs compared to background PBS controls. (**B**) Normalized relative fluorescence units (RFU) obtained from 4–6 automated images in cells treated with 10 mg/mL mCherry MNPs or Empty MNPs compared to background PBS controls. Each point represents mean ± standard deviation.

Modification of the mesoscale nanoparticle formulation to incorporate the high molecular weight hydrophilic mRNA molecule [34, 35]. To evaluate the optimal and most facile formulation method, we modulated the volume in which the mRNA was added in the primary mixture, proceeded to the nanoprecipitation step, and measured MNP size, charge, and PDI to ensure they retained the optimal mesoscale nanoparticle physicochemical characteristics [23, 24]. Particle diameter (300–425 nm) and PDI (< 0.4) were achieved with the mRNA-MNP formulation, which suggests that this formulation would also target the renal proximal tubules [23, 24]. We found that four of these formulations were within the appropriate quality control characteristics, with just incorporation of a large relative volume (0.5 mL aqueous phase in the initial mRNA mixture) giving us out-of-range formulations. Interestingly, these resulted in a smaller particle size.

Finally, we evaluated the functionality of these formulations by performing uptake and expression studies in a renal tubular epithelial cell line. We found that translation of the mCherry protein occurred in approximately one hour, similar to prior studies investigating mRNA translation timeframes [36]. We investigated the differential uptake of two concentrations, finding a robust expression in all cells evaluated with 10 mg/mL mRNA MNPs after one hour, whereas some proportion of the cells did not exhibit expression, though a majority did, for the 1 mg/mL concentration. We also found that expression of mCherry in cells treated with mCherry mRNA MNPs did decrease between 4 and 24 h, however it was still robust compared to earlier timepoints. Prior studies with mRNA LNPs found that expression was most optimal at 24 h post-transfection, however those studies also noted that this was more efficient than lipofectamine-based approaches and also subject to saturation of uptake or translation capacity of the cells [37].

This study portends the development of lipid-free and polycation-free polymeric nanoparticles for gene delivery. This may find use in ameliorating some issues with biocompatibility and controlled release of gene therapies [14, 17, 20] It also suggests that the ability to maintain formulation parameters within the mesoscale nanoparticle range portends future gene delivery specifically to the kidney for the therapy of renal diseases, though future studies are necessary to evaluate renal-specific mRNA translation *via in vivo* studies. This is supported by the use of a renal proximal tubular epithelial cell line in these studies. We found that minimal modification of the formulation process allows us to obtain mesoscale nanoparticles formulated with just polymeric components and mRNA. This will translate to the ability to deliver gene therapies directly to the kidneys for treatment of tubular-associated diseases such as acute kidney injury, chronic kidney disease, and renal cell carcinoma [38].

Conclusion

In this work, we evaluated the uptake kinetics of polymeric mesoscale nanoparticles in a renal tubular epithelial. We found that the polymeric mesoscale nanoparticle formulation was robust to the introduction of an mRNA homogenous mixture prior to nanoprecipitation. We investigated the ability of these polymeric nanoparticles to induce translation of an mCherry mRNA in the same cell line and investigated the kinetics and concentration-dependence of these *in vitro*. We anticipate these findings may be useful for gene therapeutic studies in a variety of renal diseases.

Acknowledgements The authors wish to acknowledge all members of the Williams Lab for their assistance, insight, and discussion. They also wish to acknowledge E. Jaimes (MSKCC) for insight and discussion related to the translation of MNPs. Finally, they wish to acknowledge A. Kulick (MSKCC) for a close reading of the manuscript and insightful discussion.

Funding This work was supported by the Oak Ridge Associated Universities Ralph E. Powe Junior Faculty Enhancement Award, a Professional Staff Congress of The City University of New York (PSC-CUNY) Enhanced Award, and The City College of New York Grove School of Engineering and Department of Biomedical Engineering (RMW).

Declarations

Conflict of Interest RMW is a scientific advisor with equity interest in Goldilocks Therapeutics, Inc.

References

1. Chen J, *et al*. Production and clinical development of nanoparticles for gene delivery. Molecular Therapy-Methods & Clinical Development. 2016;3:16023.
2. Hou X, *et al*. Lipid nanoparticles for mRNA delivery. Nat Rev Mater. 2021;6(12):1078–94.
3. Mitchell MJ, *et al*. Engineering precision nanoparticles for drug delivery. Nat Rev Drug Discovery. 2021;20(2):101–24.
4. Zhang MM, *et al*. The growth of siRNA-based therapeutics: Updated clinical studies. Biochem Pharmacol. 2021;189: 114432.
5. Hu B, *et al*. Therapeutic siRNA: state of the art. Signal Transduct Target Ther. 2020;5(1):1–25.
6. Hussain, A., *et al*., mRNA vaccines for COVID-19 and diverse diseases. Journal of Controlled Release, 2022.
7. Zhang, N.-N., *et al*., A thermostable mRNA vaccine against COVID-19. Cell, 2020. 182(5): p. 1271–1283. e16.
8. Walsh EE, *et al*. Safety and immunogenicity of two RNA-based Covid-19 vaccine candidates. N Engl J Med. 2020;383(25):2439–50.
9. Kim J, *et al*. Self-assembled mRNA vaccines. Adv Drug Deliv Rev. 2021;170:83–112.
10. Sahin U, Karikó K, Türeci Ö. mRNA-based therapeutics—developing a new class of drugs. Nat Rev Drug Discovery. 2014;13(10):759–80.
11. Weissman D. mRNA transcript therapy. Expert Rev Vaccines. 2015;14(2):265–81.

12. Hatit MZ, *et al*. Species-dependent in vivo mRNA delivery and cellular responses to nanoparticles. Nat Nanotechnol. 2022;17(3):310–8.
13. Demirer GS, *et al*. Nanotechnology to advance CRISPR–Cas genetic engineering of plants. Nat Nanotechnol. 2021;16(3):243–50.
14. Ashok B, Peppas NA, Wechsler ME. Lipid-and polymer-based nanoparticle systems for the delivery of CRISPR/Cas9. Journal of Drug Delivery Science and Technology. 2021;65: 102728.
15. Kulkarni JA, Cullis PR, Van Der Meel R. Lipid nanoparticles enabling gene therapies: from concepts to clinical utility. Nucleic Acid Ther. 2018;28(3):146–57.
16. Hajj KA, Whitehead KA. Tools for translation: non-viral materials for therapeutic mRNA delivery. Nat Rev Mater. 2017;2(10):1–17.
17. Bisht R, *et al*. Nanocarrier mediated retinal drug delivery: overcoming ocular barriers to treat posterior eye diseases. Wiley Interdisciplinary Reviews: Nanomedicine and Nanobiotechnology. 2018;10(2): e1473.
18. Rai R, Alwani S, Badea I. Polymeric nanoparticles in gene therapy: New avenues of design and optimization for delivery applications. Polymers. 2019;11(4):745.
19. Chen J, *et al*. Polycations for gene delivery: dilemmas and solutions. Bioconjug Chem. 2018;30(2):338–49.
20. Onoue S, Yamada S, Chan H-K. Nanodrugs: pharmacokinetics and safety. Int J Nanomed. 2014;9:1025.
21. Aied A, *et al*. Polymer gene delivery: overcoming the obstacles. Drug Discovery Today. 2013;18(21–22):1090–8.
22. Piperno A, *et al*. Recent advances and challenges in gene delivery mediated by polyester-based nanoparticles. Int J Nanomed. 2021;16:5981.
23. Williams RM, *et al*. Mesoscale nanoparticles selectively target the renal proximal tubule epithelium. Nano Lett. 2015;15(4):2358–64.
24. Williams RM, *et al*. Selective nanoparticle targeting of the renal tubules. Hypertension. 2018;71(1):87–94.
25. Williams, R.M., *et al*., Kidney-targeted redox scavenger therapy prevents cisplatin-induced acute kidney injury. Frontiers in pharmacology, 2021. 12.
26. Han, S.J., *et al*., Selective nanoparticle-mediated targeting of renal tubular Toll-like receptor 9 attenuates ischemic acute kidney injury. Kidney International, 2020.
27. Veiras, L.C., *et al*., Tubular IL-1β induces salt sensitivity in diabetes by activating renal macrophages. Circulation Research, 2022: p. https://doi.org/10.1161/CIRCRESAHA. 121.320239.
28. Benson LN, *et al*. The IFNγ-PDL1 pathway enhances CD8T-DCT interaction to promote hypertension. Circ Res. 2022;130(10):1550–64.
29. Guo X, *et al*. Kidney-targeted renalase agonist prevents cisplatin-induced chronic kidney disease by inhibiting regulated necrosis and inflammation. J Am Soc Nephrol. 2022;33(2):342–56.
30. Han, S.J., *et al*., Renal proximal tubular NEMO plays a critical role in ischemic acute kidney injury. JCI insight, 2020.
31. Schneider CA, Rasband WS, Eliceiri KW. NIH image to imagej: 25 years of image analysis. Nat Methods. 2012;9(7):671–5.
32. Vij N, *et al*. Development of PEGylated PLGA nanoparticle for controlled and sustained drug delivery in cystic fibrosis. Journal of nanobiotechnology. 2010;8(1):1–18.
33. Panyam J, *et al*. Rapid endo-lysosomal escape of poly (DL-lactide-coglycolide) nanoparticles: implications for drug and gene delivery. FASEB J. 2002;16(10):1217–26.
34. Yasar H, *et al*. Kinetics of mRNA delivery and protein translation in dendritic cells using lipid-coated PLGA nanoparticles. Journal of nanobiotechnology. 2018;16(1):1–19.
35. Park JH, *et al*. Virus-mimicking cell membrane-coated nanoparticles for cytosolic delivery of mRNA. Angew Chem. 2022;134(2): e202113671.
36. Morisaki T, Stasevich TJ. Quantifying single mRNA translation kinetics in living cells. Cold Spring Harb Perspect Biol. 2018;10(11): a032078.
37. Pardi N, *et al*. Expression kinetics of nucleoside-modified mRNA delivered in lipid nanoparticles to mice by various routes. J Control Release. 2015;217:345–51.
38. Williams RM, Jaimes EA, Heller DA. Nanomedicines for kidney diseases. Kidney Int. 2016;90(4):740–5.

Publisher's Note Springer Nature remains neutral with regard to jurisdictional claims in published maps and institutional affiliations.

Springer Nature or its licensor holds exclusive rights to this article under a publishing agreement with the author(s) or other rightsholder(s); author self-archiving of the accepted manuscript version of this article is solely governed by the terms of such publishing agreement and applicable law.